# Molybdenum Disulfide Catalytic Coatings via Atomic Layer Deposition for Solar Hydrogen Production from Copper Gallium Diselenide Photocathodes

*Thomas R. Hellstern, David W. Palm, James Carter, Alex D. DeAngelis, Kimberly Horsley, Lothar Weinhardt, Wanli Yang, Monika Blum, Nicolas Gaillard, Clemens Heske, Thomas F. Jaramillo**

Dr. T.R. Hellstern, D.W. Palm, Prof. T.F. Jaramillo*
Department of Chemical Engineering, Stanford University
443 Via Ortega, Stanford, California 94305, United States

J. Carter, Dr. L. Weinhardt, Dr. M. Blum, Prof. C. Heske
Department of Chemistry and Biochemistry, University of Nevada Las Vegas (UNLV)
4505 Maryland Pkwy, Las Vegas, Nevada 89154-4003, United States

A.D. DeAngelis, Dr. K. Horsley, Dr. N. Gaillard
Hawaii Natural Energy Institute (HNEI), University of Hawaii at Manoa
1680 East-West Rd, POST 109, Honolulu, Hawaii 96822, United States

Dr. L. Weinhardt, Prof. C. Heske
Institute for Photon Science and Synchrotron Radiation (IPS), Karlsruhe Institute of Technology (KIT)
Hermann-v.-Helmholtz-Platz 1, 76344 Eggenstein-Leopoldshafen, Germany

Institute for Chemical Technology and Polymer Chemistry (ITCP), Karlsruhe Institute of Technology (KIT)

Engesserstr. 18/20, 76128 Karlsruhe, Germany

Dr. W. Yang, Dr. M. Blum
Advanced Light Source (ALS), Lawrence Berkeley National Laboratory
1 Cyclotron Road, Berkeley, California 94720, United States

Prof. T.F. Jaramillo*
SUNCAT Center for Interface Science and Catalysis, SLAC National
Accelerator Laboratory
2575 Sand Hill Road, Menlo Park, California 94025, United States

*Corresponding Author: jaramillo@stanford.edu

KEYWORDS: Photoelectrochemical water splitting, copper gallium diselenide, molybdenum disulfide, hydrogen evolution, atomic layer deposition

ABSTRACT: We demonstrate that applying atomic layer deposition-derived molybdenum disulfide ($MoS_2$) catalytic coatings on copper gallium diselenide (CGSe) thin film absorbers can lead to efficient wide band gap photocathodes for photoelectrochemical hydrogen production. We have prepared a device that is free of precious metals, employing a CGSe absorber and a cadmium sulfide (CdS) buffer layer, a titanium dioxide ($TiO_2$) interfacial layer, and a $MoS_2$ catalytic layer. The resulting $MoS_2/TiO_2$/CdS/CGSe photocathode exhibits a photocurrent onset of +0.53 V *vs*. RHE and a saturation photocurrent density of -10 mA $cm^{-2}$, with stable operation for greater than 5 hours in acidic electrolyte. Spectroscopic investigations of this device architecture indicate that overlayer degradation occurs inhomogeneously, ultimately exposing the underlying CGSe absorber.

## Introduction

Hydrogen is an extremely important commodity chemical, used primarily for ammonia synthesis and hydrocarbon upgrading. It is produced on a scale of 65 million metric tons per year.[1,2] Steam reforming of natural gas is currently the dominant industrial source of hydrogen, although it emits the greenhouse gas $CO_2$ as a byproduct. Thus, more sustainable hydrogen production methods have the potential to substantially reduce greenhouse gas emissions.[3] In contrast, photoelectrochemical (PEC) water splitting, which uses sunlight and water to produce hydrogen and oxygen, offers a promising route for producing hydrogen without the direct emission of $CO_2$.[4-6] However, single-absorber PEC water splitting devices have not demonstrated suitable energy conversion efficiencies. Accordingly, numerous studies have recommended the use of stacked dual-absorber PEC water splitting devices, because this configuration can achieve higher solar-to-hydrogen (STH) efficiencies.[6-10]

A key challenge in implementing an efficient dual-absorber PEC water splitting device is the development of a wide band gap photoelectrode that (1) has a band gap between 1.6 and 1.8 eV, optimal for current and voltage output to split water when paired with a smaller band gap photoelectrode, and (2) maintains long-term, stable operation.[5,11] The copper indium gallium diselenide ($CuIn_{1-x}Ga_xSe_2$ or CIGSe) chalcopyrite system contains promising candidates for photoabsorbers due to high demonstrated photovoltaic conversion efficiency,[12,13] low-cost deposition methods,[14, 15] and a compositionally-tunable band gap.[16]

Copper gallium diselenide ($CuGaSe_2$ or CGSe) has the widest band gap (~1.7 eV) of the CIGSe material class and has been previously used as a p-type absorber in PEC systems.[17-20] However, the CGSe band edges do not align with the hydrogen and oxygen evolution redox potentials, which leads to a poor onset potential for the hydrogen evolution reaction (HER).[19] In order to overcome this limitation, cadmium sulfide (CdS) has been employed as a buffer layer to improve the photovoltage and therefore the onset potential for HER.[17,18,21] Unfortunately, CdS has been shown to be highly unstable under illumination in aqueous conditions.[22,23] Although work has been done on the durability of CdS/CGSe electrodes in neutral conditions, operation of a water splitting device at pH = 7 may introduce additional challenges due to the formation of pH gradients.[18,24] Hence, there is incentive to develop catalytic schemes that extend the operation of CdS/CGSe for splitting water in acidic or basic electrolyte.

Molybdenum sulfides are promising catalytic layers for CdS/CGSe for several reasons. $MoS_2$ thin films have demonstrated excellent stability in acidic electrolytes and have enhanced the durability of silicon and III-V semiconductor photocathodes.[25-30] The edge sites of $MoS_2$ are also some of the most active non-precious-metal hydrogen evolution catalyst sites, on a turnover frequency basis.[31,32] To date, $MoS_2$ catalytic layers for photoelectrodes have only been formed from sputtered films of molybdenum or by electrodeposition. We have developed a new method to deposit extremely thin, low light absorbing $MoS_2$-based schemes via low temperature

atomic layer deposition (ALD). Here, we report on their activity, durability, and degradation mechanisms when integrated with CdS/CGSe photoelectrodes.

In particular: (1) we have integrated thin films of $MoS_2$ and $TiO_2$ deposited via ALD to serve as a catalytic scheme for polycrystalline, rough films of CdS/CGSe. (2) We have investigated the electrochemical activity and durability of the resulting $MoS_2/TiO_2$/CdS/CGSe photocathode. (3) We have performed soft x-ray spectroscopy to gain insight into the degradation mechanisms of the $MoS_2/TiO_2$/CdS/CGSe photocathode.

## Experimental Methods

### *Device Fabrication*

CGSe films were deposited on clean soda-lime glass coated with 400 nm of fluorine-doped tin oxide (FTO substrates, Hartford City Glass, TEC 15, 15 Ω/sq.). FTO substrates were cleaned by sonicating them in alconox solution (2 wt. %), acetone, then methanol, each for 5 minutes. Substrates were thoroughly rinsed in de-ionized (DI) water between each sonication step. The films were deposited by a three-stage co-evaporation process[33] modified to yield $CuGaSe_2$, which has been shown to make a good ohmic contact to the FTO.[34] In the first stage, gallium (1.5 Å/s) and selenium (20.0 Å/s) were co-evaporated onto the substrates at a nominal substrate temperature ($T_{sub}$) of 420°C. In the second stage, copper (1.0 Å/s) and selenium were deposited at a $T_{sub}$ of 580°C. Copper continued to be deposited such that a decrease in temperature of 3-10°C occurred after end

point detection (EPD). In the third stage, gallium and selenium were deposited once more until the substrate temperature increased back to its initial value prior to EPD. The thickness of copper and gallium was monitored during the deposition by an electron impact emission spectrometer (Guardian EIES controller, Inficon). The thickness of the CGSe films for this study was approximately 1 µm, as measured by a stylus profilometer (Alpha step 200, Tencor).

Cadmium sulfide (CdS) was deposited on CGSe by chemical bath deposition (CBD), following the recipe described in Ref. 22. In short, a 50 mL CBD solution was made in a reaction vessel containing 5 mL of 1.5 M cadmium sulfate 8/3 hydrate (Sigma) solution, 6.25 mL of 30% ammonium hydroxide solution (Fisher), 2.5 mL of 1.5 M thiourea (Sigma) solution, and 36.25 mL of DI water. The vessel was heated to 65°C by placing it into a recirculating water bath that was preheated to this temperature. CGSe samples were suspended in the reaction vessel, and the reaction was allowed to proceed for 10-12 minutes. Samples were removed, washed in DI water, and dried immediately with air before transporting to a cleanroom environment for further deposition. Cadmium sulfide is toxic and cadmium compounds are known carcinogens; as such, all CdS depositions were performed in a specified area in a fume hood, and all waste created in the process was handled and stored separately from other laboratory waste.

$TiO_2$ was deposited using ALD as previously described,[35] using tetrakis(dimethylamido)titanium(IV) (TDMA-Ti) from Strem and DI water as

precursors in a Cambridge Nanotech Savannah ALD reactor at 150°C. Saturated linear growth was observed with a growth rate of 0.45 - 0.50 Å/cycle. The TDMA-Ti precursor was heated to 75°C for deposition and 5 nm of $TiO_2$ was deposited over 100 cycles. After $TiO_2$ deposition, the sample was transferred directly to the next ALD reactor for $MoO_x$ deposition.

$MoO_x$ was deposited using ALD parameters adapted from previous reports.[36] Unlike in previous studies, $MoO_x$ was deposited using molybdenum hexacarbonyl ($Mo(CO)_6$) and oxygen plasma in a Cambridge Nanotech Fiji ALD reactor at 165°C. Saturated linear growth was observed with a growth rate of nearly 0.6 Å/cycle, as shown in **Figure S1**. The $Mo(CO)_6$ precursor was heated to 70°C for deposition and 4.5 nm of $MoO_x$ was deposited over 75 cycles. After $MoO_x$ deposition, the sample was transferred back to our wet-chemistry laboratory for tube furnace annealing (see below). The thicknesses of the $TiO_2$ and $MoO_x$ layers were determined using spectroscopic ellipsometry.

$MoS_2$ was synthesized by converting $MoO_x$ under flowing 10% $H_2S$ / 90% $H_2$ (approx. 10 sccm) in a tube furnace at 200°C for 30 minutes.[37] The furnace was heated to 200°C while samples were held outside of the temperature zone (at ~30°C). Samples were then inserted into the temperature zone, subsequently reaching 200°C over the course of 3.5 minutes. After 30 minutes, samples were removed from the temperature zone and allowed to rapidly cool. Hydrogen sulfide ($H_2S$) is a highly toxic and

flammable gas, which must only be used and stored inside a ventilated fume hood. We test for $H_2S$ leaks in our tube furnace setup using an RKI Instruments GX-2009 Portable Multi Gas Detector and scrub the effluent gas (forming CuS) using a glass bubbler containing aqueous hydrogen peroxide solution (30%) and copper wire.

*Spectroscopic and Microscopic characterization*

X-ray Photoelectron Spectroscopy (XPS) and X-ray excited Auger Electron Spectroscopy (XAES) were performed at UNLV using a modified VG ESCALab MkII with a SPECS PHOIBOS 150 MCD electron analyzer and a SPECS XR-50 dual anode X-ray source. Sulfur $L_{2,3}$ X-ray Emission Spectroscopy (XES) data was obtained at Beamline 8.0.1 of the Advanced Light Source (ALS), Lawrence Berkeley National Laboratory, using the newly installed iRIXS endstation (8.0.1.1).[38] After preparation and testing at Stanford, the samples were packaged in a dry nitrogen environment and transferred to UNLV. The packaging was opened in an $N_2$-filled glove box, and samples were mounted and transferred into ultra-high vacuum (UHV) without air exposure. For subsequent measurements at the ALS, the samples were repackaged in the glove box and transferred to the ALS in Berkeley. Some samples were directly transferred from Stanford to the ALS. Before transfer into the iRIXS chamber at the ALS, samples were briefly (< 5 min) exposed to air.

SEM was performed using a FEI Magellan 400 XHR at the Stanford Nano Shared Facility (SNSF). Optical transmission measurements were performed using a Varian Cary 6000i UV-Vis-NIR spectrophotometer at the Stanford Soft Materials Facility (SMF). Optical absorption measurements were performed using an integrating sphere with white light from a 1000 W xenon lamp. Light was directed onto the sample and unabsorbed light was collected and measured using an Ocean Optics Jaz EL 200-XR1 spectrometer. X-ray diffraction measurements were performed using a Philips PANalytical X'Pert Pro in parallel beam mode with Cu $K_\alpha$ radiation.

*Photoelectrochemical Characterization*

The CdS/CGSe photocathodes were prepared by first physically removing part of the CGSe film from the FTO substrate using a razor blade and then making electrical contact to the exposed FTO using conductive carbon paint (DAG-T-502). A tinned copper insulated hookup wire (Belden 8502-009) was attached using the carbon paint, which was then allowed to dry for 10 minutes. The electrodes were mounted using inert epoxy (Loctite Hysol 9462) and allowed to cure overnight before testing. The active area of each sample was measured using a photograph and image analysis software (ImageJ); measured working electrode areas ranged from 0.15 to 0.3 $cm^2$.

PEC measurements[39] were performed in a three-electrode cell configuration using a Bio-Logic potentiostat (VSP) and a two-compartment glass cell separated by a proton-conducting Nafion membrane. The CdS/CGSe working electrode and $Hg/Hg_2SO_4$ (saturated $K_2SO_4$) reference

electrode were placed in one compartment, while an $IrO_x$/Ir wire counter electrode was placed in the other compartment to minimize contamination. The front of the working electrode was illuminated through a fused silica window. In order to dissolve hydrogen gas and displace dissolved oxygen, the working electrode compartment was purged with $H_2$ for at least 10 minutes prior to the cyclic voltammetry measurements, and during the course of the 24 hr chronoamperometry (CA) stability measurements. The reference electrode was calibrated to the reversible hydrogen electrode (RHE) scale by measuring the redox potential for the $H^+/H_2$ couple using platinum working and counter electrodes in $H_2$-purged 0.5 M $H_2SO_4$ electrolyte.

The performance of the CdS/CGSe photocathodes was assessed by performing linear sweep voltammetry (LSV) from -0.55 V *vs.* RHE to approximately 0.2 V positive of the onset potential at 10 mV $s^{-1}$. The onset potentials reported in this study were determined by a linear extrapolation of the LSV's main photocurrent onset feature to its intersection with the j = 0 axis. The potential at which this intersection occurs is defined as the onset potential for the purposes of this study, similar to previously reported methods.[34] A graphical demonstration of this procedure is included in **Figure S2**. The stability of the CdS/CGSe photocathode was assessed by performing (1) an initial illuminated LSV, in the potential range described above, (2) a dark LSV between 0.0 V and -0.55 V *vs.* RHE at 10 mV $s^{-1}$, (3) a CA

measurement held at 0.0 V *vs.* RHE for 24 hrs, and (4), (5) final illuminated and dark LSVs, respectively.

The light source used for 1-Sun PEC testing was a 150 W Xe arc lamp. The irradiance was measured using an Ocean Optics Jaz EL 200-XR1 spectrometer and calibrated to match the AM1.5G solar spectrum. Details about the calibration procedure are described in the supporting information. The light source used for incident photon-to-current conversion efficiency (IPCE) measurements was a 1000 W Hg/Xe arc lamp, in conjunction with a Newport Oriel 74100 monochromator. The spectral output of the lamp/monochromator assembly was measured using the Ocean Optics Jaz spectrometer listed above.

## Results and Discussion

### *Synthesis of $MoS_2$/$TiO_2$/CdS/CGSe photocathodes*

A schematic diagram and SEM images of a $MoS_2$/$TiO_2$/CdS/CGSe/FTO/glass photocathode are shown in **Figure 1**. X-ray diffraction of CGSe electrodes, as shown in **Figure S3**, confirms the chalcopyrite crystal phase. An FTO substrate was used to ensure optical transmission of below band gap photons (Figure S4), an important quality for creating a stacked tandem PEC water splitting device.

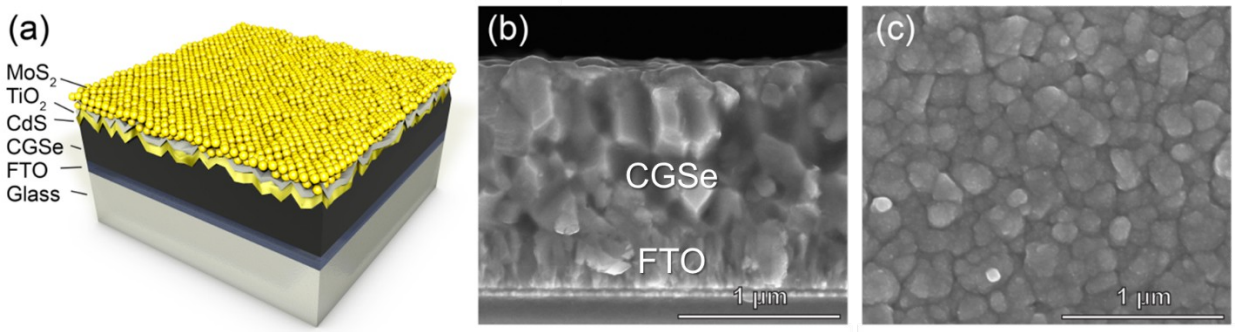


**Figure 1:** (a) Schematic, (b) cross-sectional SEM image, and (c) top view SEM image of $MoS_2/TiO_2/CdS/CGSe$ photocathode on FTO. $MoS_2$, $TiO_2$, and CdS layers are thin and cannot be distinguished in the cross-section. SEM images also show the grain size distribution of CGSe.

As shown in **Figure 2a**, the best photocurrent onset was achieved when the buffer and both the $MoS_2$ and $TiO_2$ layers were included. The onset potential for the bare CGSe electrode was found at only +0.02 V *vs.* RHE, likely due to poor band alignment relative to the reversible hydrogen potential.[19] In order to overcome the limitations of the CGSe-electrolyte junction, a CdS buffer layer was deposited by CBD to create a solid-state junction analogous to those widely used in CIGSe photovoltaic devices.[21,40] With the addition of CdS, the onset improved to +0.12 V *vs.* RHE, a modest increase with room for improvement since CdS is a poor catalyst for HER The onset was further improved by the addition of a $MoS_2$ catalytic layer, reaching +0.35 V *vs*. RHE. Furthermore, the treatment time and temperature utilized during the formation of $MoS_2$ from $MoO_x$ in sulfurous atmosphere were optimized for catalytic performance, transparency, and durability, and utilizing $TiO_2$ as an additional interfacial layer demonstrated further enhanced performance (**Figures S5-7**). This optimized $MoS_2/TiO_2/CdS/CGSe$

photocathode showed an onset of +0.53 V *vs*. RHE and achieved a photocurrent density of -10 mA $cm^{-2}$ at -0.5 V *vs.* RHE (Figure 2a). In addition, a maximum IPCE of 0.53 was achieved for this device under bias of -0.5 V *vs*. RHE and a maximum IPCE of 0.44 was achieved at 0 V *vs*. RHE (**Figure 2b)**.

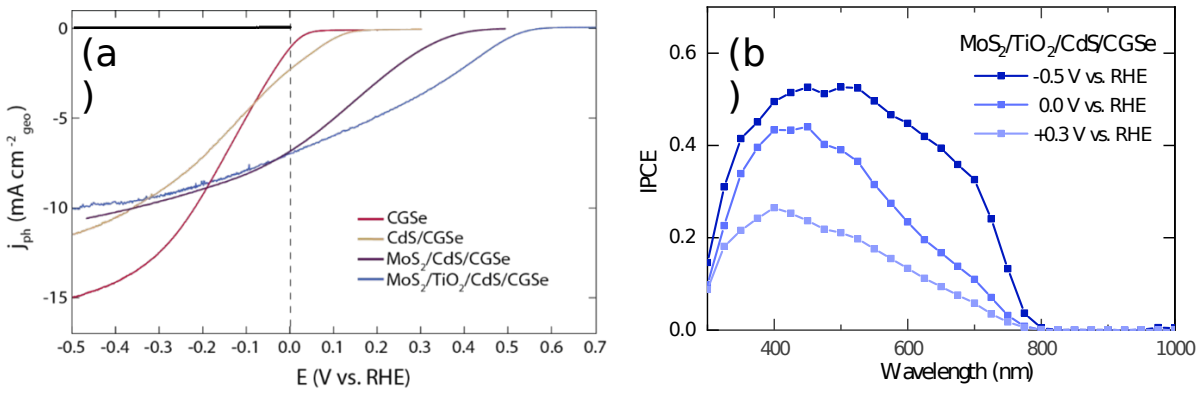


**Figure 2:** (a) PEC activity of the bare CGSe (red), CdS/CGSe (gold), $MoS_2$/CdS/CGSe (purple), and $MoS_2$/$TiO_2$/CdS/CGSe (blue) samples tested under AM1.5G illumination; the dark LSV for the $MoS_2$/CdS/CGSe sample (typical of all samples) is shown in black for reference. (b) Incident photon-to-current conversion efficiency (IPCE) of the $MoS_2$/$TiO_2$/CdS/CGSe device at various applied potentials. All electrodes were tested in $H_2$-sparged 0.5 M $H_2SO_4$ electrolyte with a Hg/$HgSO_4$ reference electrode and an Ir/$IrO_x$ counter electrode.

*Assessing the durability of $MoS_2$/$TiO_2$/CdS/CGSe photocathodes*

In order to evaluate PEC durability of the $MoS_2$/$TiO_2$/CdS/CGSe photocathode, CA tests were conducted in which the potential was maintained at 0 V *vs.* RHE for 24 hrs under constant illumination, with LSVs were performed at 0 and 24 hrs. Hydrogen production is the dominant contributor to the photocurrent generated over the course of the experiment, given the sustained bubble formation at the electrode surface, the substantial total charge passed ($10^{-3}$ mol $e^-$, calculated in the Supporting

Information), and the well-documented high Faradaic efficiencies for $H_2$ evolution on $MoS_2$ catalysts.[29] An identically-prepared sample was tested in this manner for 7 hrs and then characterized to gain insight into the chemical changes occurring at the photocathode surface over the course of electrochemical testing. **Figure 3** shows (a) LSVs at 0, 7, and 24 hr time intervals, and (b) CA stability data (at 0.0 V *vs*. RHE) over 24 hrs.

During the LSVs in **Figure 3a**, this $MoS_2/TiO_2$/CdS/CGSe photocathode tested at 0 hrs showed an onset potential of +0.53 V vs. RHE, and achieved an approximate saturation photocurrent density of -10 mA $cm^{-2}$; the maximum dark current over the measured potential range was -0.02 mA $cm^{-2}$ (Figure 3a). After 7 hrs of testing, the onset potential shifted to +0.25 V *vs.* RHE, with the shape of the LSV changing significantly. After 24 hrs of testing, the onset potential shifted to -0.05 V *vs*. RHE and the shape of the curve again changed substantially to resemble that of the bare CGSe electrode shown in Figure 2. The saturation photocurrent density of the electrode also increased after 24 hrs of testing, consistent with a thinning of the CdS layer, which parasitically absorbs incident light (**Figure S7**). The CA measurement in **Figure 3b** indicates that the electrode current density is stable for approximately 5 hrs at -6.5 mA $cm^{-2}$, before degrading to -2 mA $cm^{-2}$ after 15 hrs. The maximum dark current increases steadily to a final value of -0.09 mA $cm^{-2}$ after 24 hrs of durability testing, as shown in Figure S8.

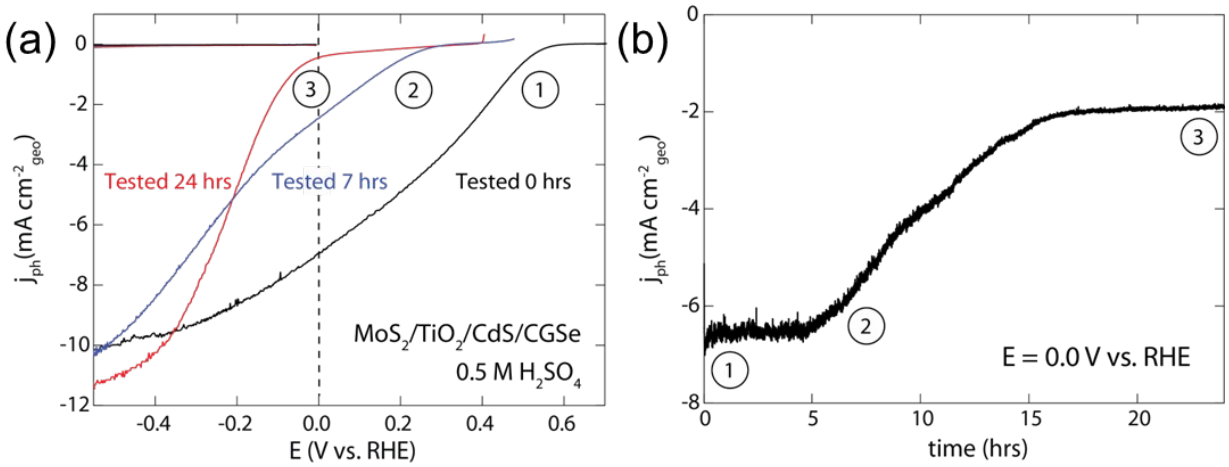


322

323**Figure 3:** (a) LSVs of $MoS_2/TiO_2$/CdS/CGSe photocathodes as prepared 324(black), after 7 hrs stability testing (blue), and after 24 hrs of stability testing 325(red). The corresponding dark scans are also shown. (b) A 24 hr stability test 326tracking the current density at 0.0 V *vs.* RHE. LSV time points from (a) are 327marked (1-3). Tests performed under simulated AM1.5G illumination.

328

329*Spectroscopic investigation of degradation in $MoS_2/TiO_2$/CdS/CGSe*

330*photocathodes*

331 We performed spectroscopic studies of the as-prepared and tested 332photoelectrodes and combined this information with the preceding 333photoelectrochemical data in order to understand the device degradation. 334From this combination of techniques, it is evident that significant changes in 335surface composition occurred during the testing process. We postulate that 336device deterioration occurs as the electrolyte infiltrates and dissolves the 337$MoS_2/TiO_2$ films and the underlying CdS due to instabilities in acidic media.

338 **Figure 4a** shows an XPS survey of the shallow core levels, while 339**Figures 4b, 4c,** and **4d** depict the Cd 3d/Mo 3p/Ga LMM XPS and XAES 340spectra, the Ti 2p XPS spectra, and the S $L_{2,3}$ XES spectra, respectively. The 341surface-sensitive XPS spectra (Figures 4a-c) show that the as-prepared

sample surface ("Tested 0 hrs") was dominated by the $MoS_2/TiO_2$ dual layer, while the sample surface after 7 hrs of testing exhibits a mixture of chemical environments, showing strong characteristic peaks for S, Cd, and Mo, as well as weaker signals for Ti, Cu, Se, and Ga. After 24 hours of testing, the XPS signals primarily resemble those of a CGSe surface. Furthermore, the S $L_{2,3}$ XES spectra (Figure 4d), with significantly larger attenuation depth, show the presence of a CdS chemical environment in the film (in particular the Cd 4d-derived peaks[41,42] labeled (b)) for the 0 and 7 hrs-tested samples. In comparison to the CdS reference, the upper valence band feature labeled (c) shows a slightly more symmetric spectral shape and is shifted to higher emission energies, possibly indicative of spectral contributions from S in a $MoS_2$ chemical environment. In contrast, the S signal is completely removed after 24 hours of testing, and only a broad Se $M_{2,3}$ peak at 148 eV is observed.[43]

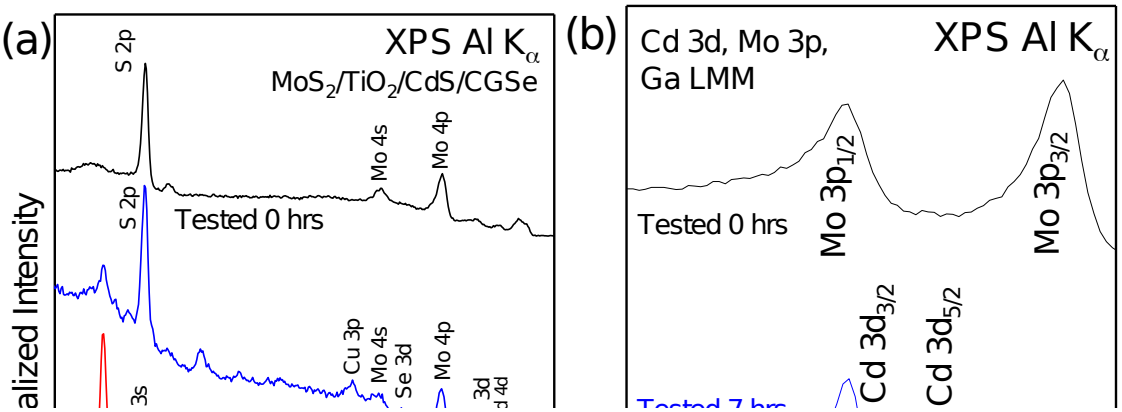


We posit that, during the degradation processes, the surface of the electrode was composed of regions of $MoS_2/TiO_2$, exposed CdS, as well as bare CGSe. This model agrees with the XPS data taken at 7 hrs (Figures 4a

and 4c) and the LSV after 7 hrs of testing in Figure 3a, where the more positive onset potential compared to that of the bare CGSe (Figure 2) is evidence that some portion of the CdS/CGSe junction and the associated catalytic overlayers remained intact. This suggests that the degradation process is inhomogeneous and may involve multiple mechanisms. After 24 hrs of testing, significant degradation of the overlayers had occurred, as evidenced by the similarity of both the LSV and spectroscopic scans to those of the bare CGSe absorber electrode, with similar onset potential but slightly lower saturation photocurrent density.

**Conclusions**

A low-temperature scheme (< 200°C) was developed using ALD to synthesize $MoS_2/TiO_2$ overlayers for photocathodes. Combining insights from electrochemical and spectroscopic characterization, we determined that: (1) $MoS_2/TiO_2$ can serve as an effective catalytic scheme for CdS/CGSe photocathodes, (2) these overlayers provided only short-term protection from the acidic electrolyte, and (3) the degradation process is inhomogeneous and likely occurs through multiple pathways, ultimately exposing the underlying CGSe absorber. Building on these findings, the overlayer synthesis developed here can be further optimized and also generalized to other material systems that are constrained by sensitivity to temperature. Improvements in activity and durability for CdS/CGSe photocathodes would facilitate the development of promising tandem

schemes for unassisted water splitting, and further work to disentangle the complex degradation pathways and interfacial energetics would accelerate such developments.

**Acknowledgments**

The work was funded by the Department of Energy (DOE) under contract no. DE-EE0006670, administrated by the University of Hawaii. This research used resources of the Advanced Light Source, which is a DOE Office of Science User Facility under contract no. DE-AC02-05CH11231. Fundamental catalyst development was supported by the U.S. Department of Energy, Chemical Sciences, Geosciences, and Biosciences (CSGB) Division of the Office of Basic Energy Sciences, via Grant DE-AC02-76SF00515 to the SUNCAT Center for Interface Science and Catalysis. Part of this work was performed at the Stanford Nano Shared Facilities (SNSF), supported by the National Science Foundation under award ECCS-1542152. Part of this work was also conducted at the Stanford Nanofabrication Facility (SNF) with guidance from their staff, especially Dr. Michelle Rincon. Thank you to Dr. Pongkarn Chakthranont for contributing the three-dimensional device schematic. Finally, TRH and DWP would like to thank the National Science Foundation for its support through the Graduate Research Fellowship Program.

405*Supporting Information*. Additional details regarding calibration, data
406analysis, and material synthesis and characterization can be found in the
407Supporting Information.

408

409**References**

410


4111. Häussinger, P.; Lohmüller, R.; Watson, A. M.. Hydrogen, 6. Uses. In
412*Ullmann's Encyclopedia of Industrial Chemistry*, Wiley-VCH: Weinheim,
413Germany, 2000.
4142. Badwal, S. P.; Giddey, S.; Munnings, C. Hydrogen production via solid
415electrolytic routes. *Wiley Interdisciplinary Reviews: Energy and Environment*
416**2013,** *2*, 473-487.
4173. Kim, J. W.; Boo, K. J.; Cho, J. H.; Moon, I. 1 - Key challenges in the
418development of an infrastructure for hydrogen production, delivery, storage
419and use. In *Advances in Hydrogen Production, Storage and Distribution*;
420Basile, A.; Iulianelli, A., Eds; Woodhead: Sawston, UK, 2014; pp 3-31.
4214. Bak, T.; Nowotny, J.; Rekas, M.; Sorrell, C. C. Photo-electrochemical
422hydrogen generation from water using solar energy. Materials-related
423aspects. *International Journal of Hydrogen Energy* **2002,** *27*, 991-1022.
4245. Pinaud, B. A.; Benck, J. D.; Seitz, L. C.; Forman, A. J.; Chen, Z. B.;
425Deutsch, T. G.; James, B. D.; Baum, K. N.; Baum, G. N.; Ardo, S.; Wang, H. L.;
426Miller, E.; Jaramillo, T. F. Technical and economic feasibility of centralized
427facilities for solar hydrogen production *via* photocatalysis and
428photoelectrochemistry. *Energy & Environmental Science* **2013,** *6*, 1983-
4292002.
4306. Walter, M. G.; Warren, E. L.; McKone, J. R.; Boettcher, S. W.; Mi, Q. X.;
431Santori, E. A.; Lewis, N. S. Solar Water Splitting Cells. *Chemical Reviews*
432**2010,** *110*, 6446-6473.
4337. Seitz, L. C.; Chen, Z.; Forman, A. J.; Pinaud, B. A.; Benck, J. D.; Jaramillo,
434T. F. Modeling Practical Performance Limits of Photoelectrochemical Water
435Splitting Based on the Current State of Materials Research. *ChemSusChem*
436**2014,** *7*, 1372-85.
4378. Hu, S.; Xiang, C. X.; Haussener, S.; Berger, A. D.; Lewis, N. S. An
438analysis of the optimal band gaps of light absorbers in integrated tandem
439photoelectrochemical water-splitting systems. *Energy & Environmental*
440*Science* **2013,** *6*, 2984-2993.
4419. Weber, M. F.; Dignam, M. J. Efficiency of Splitting Water with
442Semiconducting Photoelectrodes. *Journal of the Electrochemical Society*
443**1984,** *131*, 1258-1265.
44410. Doscher, H.; Geisz, J. F.; Deutsch, T. G.; Turner, J. A. Sunlight
445absorption in water—efficiency and design implications for

photoelectrochemical devices. *Energy & Environmental Science* **2014,** *7*, 2951-2956.

11. Shaner, M. R.; Atwater, H. A.; Lewis, N. S.; McFarland, E. W. A comparative technoeconomic analysis of renewable hydrogen production using solar energy. *Energy & Environmental Science* **2016,** *9*, 2354-2371.

12. Young, D. L.; Keane, J.; Duda, A.; AbuShama, J. A.; Perkins, C. L.; Romero, M.; Noufi, R. Improved performance in ZnO/CdS/$CuGaSe_2$ thin-film solar cells. *Progress in Photovoltaics: Research and Applications* **2003,** *11*, 535-541.

13. Powalla, M.; Witte, W.; Jackson, P.; Paetel, S.; Lotter, E.; Wuerz, R.; Kessler, F.; Tschamber, C.; Hempel, W.; Hariskos, D.; Menner, R.; Bauer, A.; Spiering, S.; Ahlswede, E.; Friedlmeier, T. M.; Blázquez-Sánchez, D.; Klugius, I.; Wischmann, W. CIGS Cells and Modules with High Efficiency on Glass and Flexible Substrates. *IEEE Journal of Photovoltaics* **2014,** *4*, 440-446.

14. Panthani, M. G.; Akhavan, V.; Goodfellow, B.; Schmidtke, J. P.; Dunn, L.; Dodabalapur, A.; Barbara, P. F.; Korgel, B. A. Synthesis of $CuInS_2$, $CuInSe_2$, and $Cu(In_xGa_{1-x})Se_2$ (CIGS) Nanocrystal 'Inks' for Printable Photovoltaics. *Journal of the American Chemical Society* **2008,** *130*, 16770-16777.

15. Uhl, A. R.; Katahara, J. K.; Hillhouse, H. W. Molecular-ink route to 13.0% efficient low-bandgap $CuIn(S,Se)_2$ and 14.7% efficient $Cu(In,Ga)(S,Se)_2$ solar cells. *Energy & Environmental Science* **2016,** *9*, 130-134.

16. Bär, M.; Bohne, W.; Röhrich, J.; Strub, E.; Lindner, S.; Lux-Steiner, M. C.; Fischer, C.-H.; Niesen, T. P.; Karg, F. Determination of the band gap depth profile of the penternary $Cu(In_{(1-X)}Ga_X(S_YSe_{(1-Y)})_2$ chalcopyrite from its composition gradient. *Journal of Applied Physics* **2004,** *96*, 3857-3860.

17. Kumagai, H.; Minegishi, T.; Moriya, Y.; Kubota, J.; Domen, K. Photoelectrochemical Hydrogen Evolution from Water Using Copper Gallium Selenide Electrodes Prepared by a Particle Transfer Method. *The Journal of Physical Chemistry C* **2014,** *118*, 16386-16392.

18. Moriya, M.; Minegishi, T.; Kumagai, H.; Katayama, M.; Kubota, J.; Domen, K. Stable Hydrogen Evolution from CdS-Modified $CuGaSe_2$ Photoelectrode under Visible-Light Irradiation. *Journal of the American Chemical Society* **2013,** *135*, 3733-3735.

19. Marsen, B.; Cole, B.; Miller, E. L. Photoelectrolysis of water using thin copper gallium diselenide electrodes. *Solar Energy Materials and Solar Cells* **2008,** *92*, 1054-1058.

20. Kaneshiro, J.; Gaillard, N.; Rocheleau, R.; Miller, E. Advances in copper-chalcopyrite thin films for solar energy conversion. *Solar Energy Materials and Solar Cells* **2010,** *94*, 12-16.

21. Naghavi, N.; Abou-Ras, D.; Allsop, N.; Barreau, N.; Bücheler, S.; Ennaoui, A.; Fischer, C. H.; Guillen, C.; Hariskos, D.; Herrero, J. Buffer layers and transparent conducting oxides for chalcopyrite $Cu(In,Ga)(S,Se)_2$ based thin film photovoltaics: present status and current developments. *Progress in Photovoltaics: Research and Applications* **2010,** *18*, 411-433.

49022. Inoue, T.; Watanabe, T.; Fujishima, A.; Honda, K. i.; Kohayakawa, K. 491Suppression of surface dissolution of CdS photoanode by reducing agents. 492*Journal of The Electrochemical Society* **1977,** *124*, 719-722.
49323. Gerischer, H. On the stability of semiconductor electrodes against 494photodecomposition. *Journal of Electroanalytical Chemistry and Interfacial* 495*Electrochemistry* **1977,** *82*, 133-143.
49624. Jin, J.; Walczak, K.; Singh, M. R.; Karp, C.; Lewis, N. S.; Xiang, C. X. An 497experimental and modeling/simulation-based evaluation of the efficiency and 498operational performance characteristics of an integrated, membrane-free, 499neutral pH solar-driven water-splitting system. *Energy & Environmental* 500*Science* **2014,** *7*, 3371-3380.
50125. Benck, J. D.; Lee, S. C.; Fong, K. D.; Kibsgaard, J.; Sinclair, R.; Jaramillo, 502T. F. Designing Active and Atable Silicon Photocathodes for Solar Hydrogen 503Production Using Molybdenum Sulfide Nanomaterials. *Advanced Energy* 504*Materials* **2014,** *4*, 1400739.
50526. Britto, R. J.; Benck, J. D.; Young, J. L.; Hahn, C.; Deutsch, T. G.; Jaramillo, 506T. F. Molybdenum Disulfide as a Protection Layer and Catalyst for Gallium 507Indium Phosphide Solar Water Splitting Photocathodes. *The Journal of* 508*Physical Chemistry Letters* **2016,** *7*, 2044-2049.
50927. Gu, J.; Aguiar, J. A.; Ferrere, S.; Steirer, K. X.; Yan, Y.; Xiao, C.; Young, 510James L.; Al-Jassim, M.; Neale, N. R.; Turner, J. A. A graded catalytic-511protective layer for an efficient and stable water-splitting photocathode. 512*Nature Energy* **2017,** *2*, 16192.
51328. King, L. A.; Hellstern, T. R.; Park, J.; Sinclair, R.; Jaramillo, T. F. Highly 514Stable Molybdenum Disulfide Protected Silicon Photocathodes for 515Photoelectrochemical Water Splitting. *ACS Appl. Mater. Interfaces* **2017**, *9*, 51636792-36798.
51729. Morales-Guio, C. G.; Tilley, S. D.; Vrubel, H.; Grätzel, M.; Hu, X. 518"Hydrogen evolution from a copper (I) oxide photocathode coated with and 519amorphous molybdenum sulphide catalyst" *Nature Communications* **2014,** 5205, 3059.
52130. Laursen, A. B.; Pedersen, T.; Malacrida, P.; Seger, B.; Hansen, O.; 522Vesborg, P. C. K.; Chorkendorff, I. $MoS_2$—an integrated protective and active 523layer on $n^+p$-Si for solar $H_2$ evolution. *Phys. Chem. Chem. Phys.* **2013,** *15*, 52420000-20004.
52531. Benck, J. D.; Hellstern, T. R.; Kibsgaard, J.; Chakthranont, P.; Jaramillo, 526T. F. Catalyzing the Hydrogen Evolution Reaction (HER) with Molybdenum 527Sulfide Nanomaterials. *ACS Catalysis* **2014,** *4*, 3957-3971.
52832. Jaramillo, T. F.; Jørgensen, K. P.; Bonde, J.; Nielsen, J. H.; Horch, S.; 529Chorkendorff, I. Identification of Active Edge Sites for Electrochemical $H_2$ 530Evolution from $MoS_2$ Nanocatalysts. *Science* **2007,** *317*, 100-102.
53133. Contreras, M. A.; Tuttle, J.; Gabor, A.; Tennant, A.; Ramanathan, K.; 532Asher, S.; Franz, A.; Keane, J.; Wang, L.; Scofield, J.; Noufi, R. High Efficiency 533Cu(In,Ga)$Se_2$-Based Solar Cells: Processing of Novel Absorber Structures. 534*Proceedings of 1994 IEEE 1st World Conference on Photovoltaic Energy* 535*Conversion.* **1994**, *1*, 68-75.

53634. DeAngelis, A. D.; Horsley, K.; Gaillard, N. Wide Band Gap $CuGa(S,Se)_2$
537Thin Films on Transparent Conductive Fluorinated Tin Oxide Substrates as
538Photocathode Candidates for Tandem Water Splitting Devices. *J. Phys. Chem.*
539*C* **2018**, *122*, 14304-14312.
54035. Hu, S.; Shaner, M. R.; Beardslee, J. A.; Lichterman, M.; Brunschwig, B.
541S.; Lewis, N. S. Amorphous $TiO_2$ coatings stabilize Si, GaAs, and GaP
542photoanodes for efficient water oxidation. *Science* **2014,** *344*, 1005-1009.
54336. Diskus, M.; Nilsen, O.; Fjellvag, H. Growth of thin films of molybdenum
544oxide by atomic layer deposition. *J. Mater. Chem.* **2011,** *21*, 705-710.
54537. Chen, Z.; Cummins, D.; Reinecke, B. N.; Clark, E.; Sunkara, M. K.;
546Jaramillo, T. F. Core-shell $MoO_3$-$MoS_2$ Nanowires for Hydrogen Evolution: A
547Functional Design for Electrocatalytic Materials. *Nano Letters* **2011,** *11*,
5484168-4175.
54938. Qiao, R.; Li, Q.; Zhuo, Z.; Sallis, S.; Fuchs, O.; Blum, M.; Weinhardt, L.;
550Heske, C.; Pepper, J.; Jones, M.; Brown, A.; Spucces, A.; Chow, K.; Smith, B.;
551Glans, P.-A.; Chen, Y.; Yan, S.; Pan, F.; Piper, L. F. J.; Denlinger, J.; Guo, J.;
552Hussain, Z.; Chuang, Y.-D.; Yang, W. High-efficiency *in situ* resonant inelastic
553x-ray scattering (iRIXS) endstation at the Advanced Light Source. *Review of*
554*Scientific Instruments* **2017,** *88*, 033106.
55539. Chen, Z.; Jaramillo, T. F.; Deutsch, T. G.; Kleiman-Schwarsctein, A.;
556Forman, A. J.; Gaillard, N.; Garland, R.; Takanabe, K.; Heske, C.; Sunkara, M.;
557McFarland, E. W.; Domen, K.; Miller, E. L.; Turner, J. A.; Dinh, H. N.
558Accelerating materials development for photoelectrochemical hydrogen
559production: Standards for methods, definitions, and reporting protocols. *J.*
560*Mater. Res*. **2010**, *25*, 3-16.
56140. Poortmans, J.; Arkhipov, V., *Thin film solar cells: fabrication,*
562*characterization and applications*. Wiley: New York, 2006.
56341. Weinhardt, L.; Fuchs, O.; Fleszar, A.; Bär, M.; Blum, M.; Weigand, M.;
564Denlinger, J. D.; Yang, W.; Hanke, W.; Umbach, E.; Heske, C. Resonant
565inelastic soft x-ray scattering of CdS: A two-dimensional electronic structure
566map approach. *Physical Review B* **2009,** *79*, 165305.
56742. Weinhardt, L.; Fuchs, O.; Umbach, E.; Heske, C.; Fleszar, A.; Hanke, W.;
568Denlinger, J. D. Resonant inelastic soft x-ray scattering, x-ray absorption
569spectroscopy, and density functional theory calculations of the electronic
570bulk band structure of CdS. *Physical Review B* **2007,** *75*, 165207.
57143. Pookpanratana, S.; Repins, I.; Bär, M.; Weinhardt, L.; Zhang, Y.; Félix,
572R.; Blum, M.; Yang, W.; Heske, C. CdS/$Cu(In,Ga)Se_2$ interface formation in
573high-efficiency thin film solar cells. *Applied Physics Letters* **2010,** *97*,
574074101.
575
576

577Table of Contents Graphic

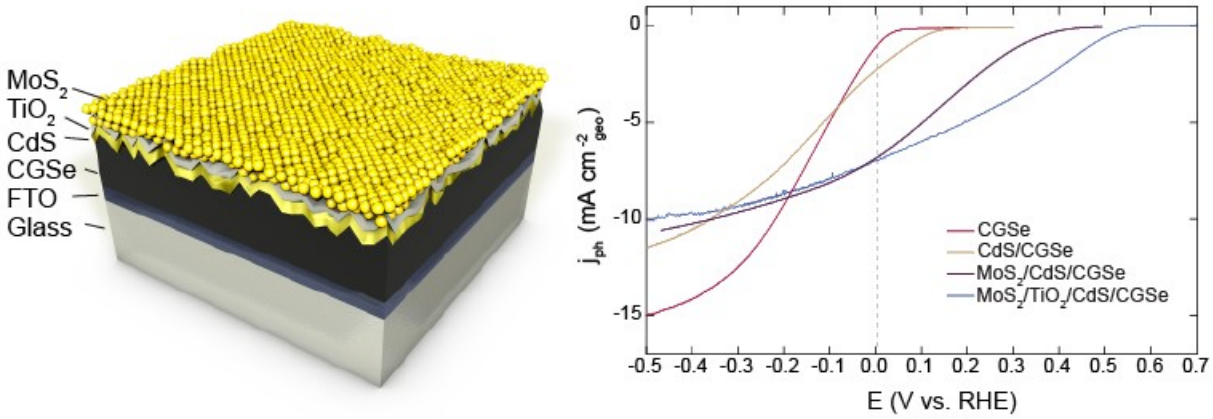


578